*Physics of the Earth and Planetary Interiors*, 9 (1974) 128–136


# FOCAL PROCESS OF THE GREAT CHILEAN EARTHQUAKE MAY 22, 1960*

HIROO KANAMORI and JOHN J. CIPAR
*Seismological Laboratory, California Institute of Technology, Pasadena, Calif. (U.S.A.)*

Accepted for publication August 27, 1974

Long-period strain seismogram recorded at Pasadena is used to determine the focal process of the 1960 Chilean earthquake. Synthetic seismograms computed for various fault models are matched with the observed strain seismogram to determine the fault parameters. A low-angle (~ 10°) thrust model with rupture length of 800 km and rupture velocity of 3.5 km/sec is consistent with the observed Rayleigh/Love wave ratio and the radiation asymmetry. A seismic moment of $2.7 \cdot 10^{30}$ dyn · cm is obtained for the main shock. This value, together with the estimated fault area of $1.6 \cdot 10^5$ km$^2$, gives an average dislocation of 24 m. The strain seismogram clearly shows unusually long-period (300–600 sec) wave arriving at the P time of a large foreshock which occurred about 15 minutes before the main shock, suggesting a large slow deformation in the epicentral area prior to the major failure. A simple dislocation model shows that a dislocation of 30 m, having a time constant of 300–600 sec, over a fault plane of 800 × 200 km$^2$ is required to explain this precursory displacement. The entire focal process may be envisaged in terms of a large-scale deformation which started rather gradually and eventually triggered the foreshocks and the "main" shock. This mechanism may explain the large premonitory deformations documented, but not recorded instrumentally, for several Japanese earthquakes. The moments of the main shock and the precursor add to $6 \cdot 10^{30}$ dyn·cm which is large enough to affect the earth's polar motion.

## 1. Introduction

The Great Chilean earthquake of May 22, 1960 ($M_S = 8.3$) is probably one of the largest earthquakes ever recorded. The free oscillations of the earth excited by this earthquake were extensively analyzed to determine the earth's eigenperiods and the attenuation property (e.g., Benioff et al., 1961; Ness et al., 1961; Alsop et al., 1961; Bogert, 1961; Alsop, 1964). On the other hand, relatively little attention has been paid to the amplitude of the free oscillations or long-period surface waves probably owing to the lack of well-calibrated long-period instrument and of theoretical basis for interpreting the amplitude data in 1960. Ben-Menahem (1971), using several published values of amplitude of free oscillations and a strain seismogram recorded at Pasadena, estimated the force system and the source intensity of this earthquake. He suggested dip-slip motion on a fault dipping 45° to the east with the oceanic side downthrown. However, in 1960, the major interest of seismologists was in the eigenperiod rather than the amplitude of free oscillations; as a result, the reported amplitude data seem to be somewhat casual. Moreover, since this earthquake occurred as a complex multiple shock and the first motion of the main shock was masked by reverberations caused by a foreshock, the focal mechanism solution is known only incompletely (Hodgson and Wickens, 1965).

Plafker (1972; see also Plafker and Savage, 1970) suggests on the basis of surface displacements of land that this earthquake represents a predominantly dip-slip movement of 20 m or more on a thrust fault inclined towards E10°S at average dip angles of about 20°. Although the geodetic data for this event are less complete than for the 1964 Alaskan earthquake, in view of its large aftershock area, efficient excitation of the lower-order free oscillations and extensive tsunamis, there is no question that this event represents truly a major tectonic process, and deserves further study; in particular, the study of long-period surface waves would reveal a more detailed picture of the physical process associated with this important event.

* Contribution No. 2509, Division of Geological and Planetary Sciences, California Institute of Technology, Pasadena, Calif.

The present paper reports analyses of long-period waves recorded by a strain seismograph at Pasadena. Although the response of this instrument was not known in detail, it recorded on-scale seismograms from the very beginning of this large event (Fig. 1). The early part of the seismogram is less susceptible to the attenuation and scattering during the propagation and is most suitable for the study of the source mechanism.

## 2. Data

Fig. 1 shows the Benioff strain seismogram recorded at Pasadena. This seismogram has been analyzed by Ben-Menahem (1965) for the study of surface-wave attenuation and by Ben-Menahem (1971) for the study of the source mechanism of the Chilean earthquake. This seismograph is a linear extensometer with a velocity transducer coupled to an over-damped (damping constant $h \sim 4$) galvanometer with a natural period $T_g$ of probably 180 sec. As shown by Benioff (1935) this system is identical, for incident waves with constant phase velocity, to an ordinary mechanical seismograph system with a pendulum period equal to $T_g$. Thus, with the strong damping ($h \sim 4$), the response at the period range of our interest (150 ~ 300 sec) is proportional to $1/T^2$ ($T$ = the period of the ground motion), and depends little on $T_g$. Therefore, the uncertainty in $T_g$ does not affect the shape of the response curve at long periods (see Fig. 2). The major unknown factor is the gain of this system which is, of course, a key parameter in the present study. Fortunately, at the time of the earthquake, Benioff long-period (pendulum period: 1 sec; galvanometer period: 90 sec), and Press-Ewing (30–90) seismograph system were operated at the same site, and we can identify distinct phases such as G4 and R4 on the seismograms recorded by these instruments. By comparing the amplitude of these waves on the strain and these calibrated instruments, we can calibrate the strain seismograph. Since the Benioff 1–90 system has a very simple and stable structure and is well calibrated, we primarily use this system to calibrate the strain seismograph. The Press-Ewing system was also calibrated occasionally, but it is a more delicate system. In particular, the vertical component is very sensitive to the drift of the zero-length spring and to a small tilt of the instrument. Thus the gain of this system is somewhat uncertain, but it can be used for cross-checking purposes. Fig. 2 shows the response curves thus calibrated basically by the Benioff 1–90 system. The magnification is probably accurate to 30% over the period range 150–300 sec.

The G2 and R2 waves on the strain seismogram (Fig. 1) are used in the present analysis. The response of the N–S strain seismograph varies as $\cos^2\phi$ and $1/2 \sin 2\phi$ for Rayleigh and Love waves respectively, where $\phi$ is the incident angle of the waves at the station measured from the north. Since $\phi \sim 325°$ for the Chile–Pasadena path, this instrument has a good sensitivity for both Rayleigh and Love waves. Because both of these waves are recorded by the same instrument, the amplitude ratio is very reliable. Ben-Menahem (1971) took advantage of this in constraining the force system.

In addition to these well defined waves, the strain seismogram shows significant long-period (5–10 minutes) waves arriving even before the expected P arrival time of the main shock. Fig. 3 shows the blow-up of this precursory long-period wave together with the Press-Ewing seismogram showing the foreshock of 18 h 55 m 57 s GMT arranged with common time axis. Judging from the noise-free quiet trace before the earthquake (see Fig. 1), this long-period precursory wave seems to represent a real signal. It is interesting to note that this precursory long-period wave follows the P and S waves of a large foreshock ($M_s$ = 6.8) which occurred about 15 minutes before the main shock (Fig. 3). It seems that a large-scale slow motion started sometime at the foreshock origin time. A brittle fracture associated with this slow process is recorded as the foreshock, and the "main shock" merely represents

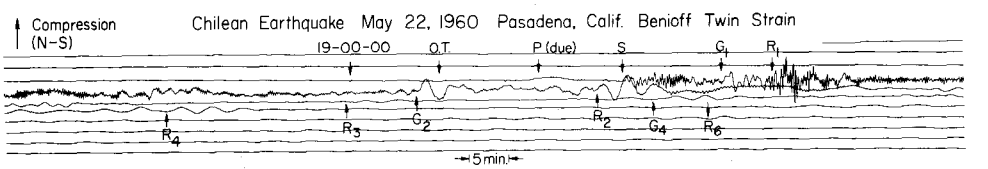


Fig. 1. Pasadena strain seismogram of the Chilean earthquake of May 22, 1960. Regular multiple surface waves are labelled. Note the long-period wave arriving before the P time.

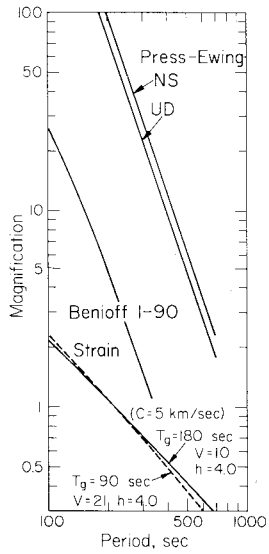


Fig. 2. Response of the strain seismograph compared with the Benioff 1–90 and the Press-Ewing system. The magnification of the strain seismograph is given for incident waves with phase velocity of 5 km/sec. For waves with phase velocity of $C$ km/sec, the magnification should be multiplied by $5/C$. The magnification curve for $T_g$ = 90 sec is also given for comparison. Note the small difference between the curves for $T_g$ = 90 and 180 sec.

another brittle fracture. Whether this long-period precursory wave is real or noise may be checked against other long-period strain records at Isabella, Nana (Benioff et al., 1961) and Ogdensberg (Alsop et al., 1961). However, on these records, because of either too slow paper speed, excessively large short-period waves resulting from the foreshock or large noise level, the identification of this wave is very difficult. The combination of the fast paper speed and the low gain of the Pasadena strain record made possible the detection of this precursory wave.

First, we will determine the source parameters of the main shock by using G2 and R2 waves. Then, we will assume that this precursory wave is real and will interpret it in relation to the main shock geometry.

## 3. Source parameters of the main shock

The source parameters of the main shock are determined by comparing the observed G2 and R2 waves with synthetic G2 and R2 computed for various source parameters. The synthetic seismograms are computed, by the procedure described in Kanamori (1970a), for the earth model 5.08 M (Kanamori, 1970b). In the present analysis, Saito's (1967) expressions are modified by using the fault representations given by Ben-Menahem et al. (1965), to obtain expressions analogous to those given by Ben-Menahem et al. (1970) for surface waves. These expressions are given in the Appendix. The numerical results agree with those by Kanamori (1970a,c) and Ben-Menahem et al. (1970).

The fault parameters concerned here are: $\delta$ = dip angle of the fault; $\phi_s$ = strike of the fault; $\lambda$ = slip angle; $M_0$ = seismic moment; $L$ = fault length; $v$ = rupture velocity; $d$ = depth. Some of these parameters seem to be constrained well by other sets of data. For example, the fault strike is well constrained by the aftershock area. We constrain $\phi_s$ at N10°E as suggested by Plafker (1972). The fault length $L$ and the rupture velocity $v$ have been estimated by Benioff et al. (1961)

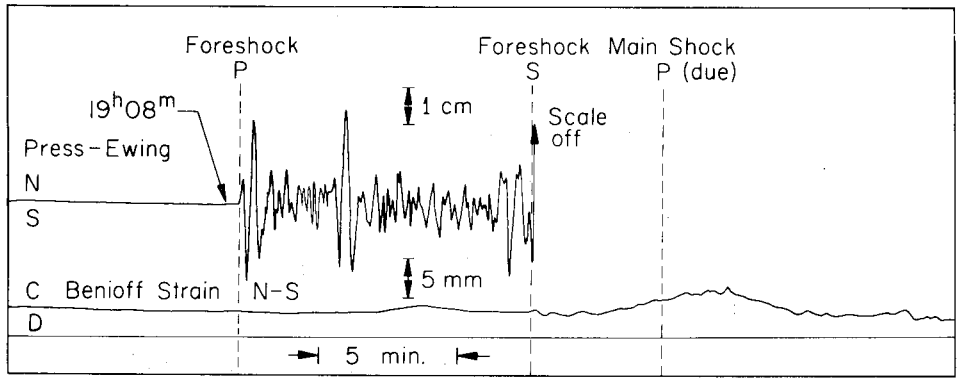


Fig. 3. Blow-up of the precursor on the strain seismogram. The Press-Ewing seismogram is shown for comparison

$\nu$ and Press et al. (1961) by using Ben-Menahem's (1961) directivity function. These authors suggest $L$ = 750 ~ 1300 km, and $\nu$ = 3 ~ 4 km/sec. Since the directivity method uses the spectral ratio of even to odd order surface waves, rather than the spectrum itself, these estimates are independent of the fault geometry. Thus it is reasonable to constrain these parameters within the above range. Several $L - \nu$ combinations are tried to see the amplitude ratio G2/G3 and R2/R3 and, to some extent, the wave form. As shown in Fig. 4, the combination of $L$ = 800 km and $\nu$ = 3.5 km/sec which is within the range given by Benioff et al. (1961) and Press et al. (1961) gives a good fit to the observed amplitude ratio. We will use these values of the rupture length and the rupture velocity throughout the present analysis.

In order to find the remaining source parameters we sweep over a wide range of $\delta$, $\lambda$ and $d$. Some of the results are given in Figs. 5 and 6 to show the sensitivity of these parameters to the synthetic seismograms and the resolution of the present method. In these figures, the synthetic seismograms computed for 5.08 M model are shifted by + 40 sec along the time axis. The propagation path of G2 and R2 includes an unusually large portion of (about 40%) tectonically active area. The synthetic seismograms computed for the model 5.08 M which represents the 'average' earth give group arrival times which are about 40 sec earlier than the observed. This difference corresponds to a difference in group velocity of approximately 0.7% which is reasonable for the

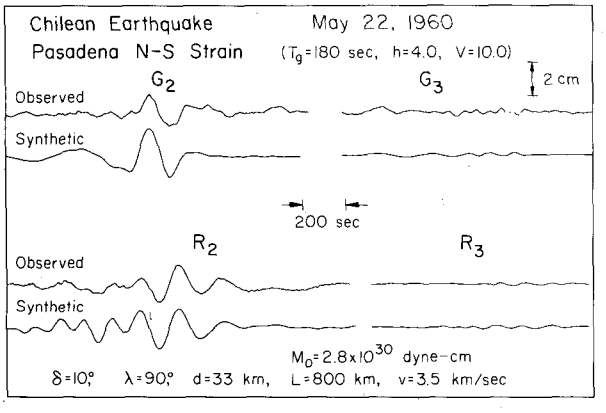


Fig. 4. Synthetic and observed seismograms for G2 vs. G3 and R2 vs. R3. The rupture length of 800 km and the rupture velocity of 3.5 km/sec are used.

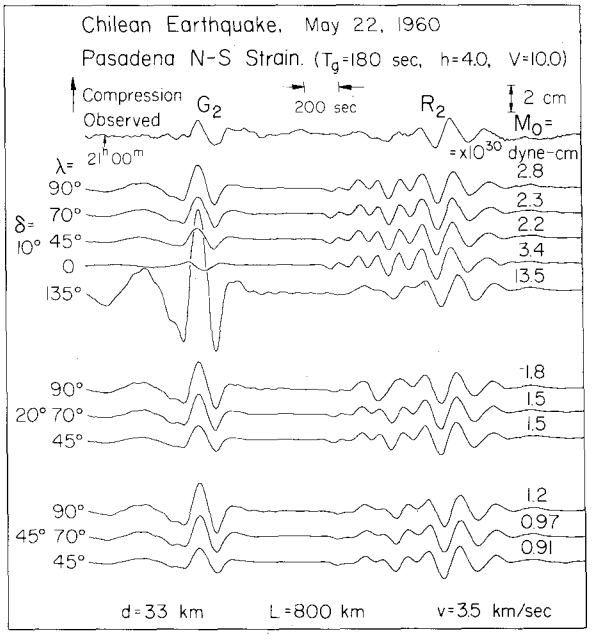


Fig. 5. Synthetic G2 and R2 for $d$ = 33 km. The dip angle and the slip angle are varied. The amplitude of R2 is normalized to the observed R2 amplitude, and the values of the seismic moment are given to each trace.

difference in the path. In Fig. 5, the source depth is fixed at 33 km while the dip angle and the slip angle are varied. The dip angle $\delta$ is measured from N100°E direction, and the slip angle is measured according to the convention given in the Appendix. As is evident for the case $\delta$ = 10°, the slip angles of 0° (pure strike-slip) and 135° (1/2 right-lateral + 1/2 thrust) do not give appropriate G2/R2 ratios. Although these cases are not shown for $\delta$ = 20° and 45°, they are also inappropriate. Thus we constrain the range of $\lambda$ to about 90° (pure thrust) to 45° (1/2 left-lateral + 1/2 thrust). It is evident from the expressions in the Appendix, eqs. 3, 4, etc. that negative slip angles which represent normal faultings give the same amplitude as that of the corresponding thrust fault, but with reversed polarity. The reverse polarity is not consistent with the observed polarity even after the 40 sec difference in the group arrival time is allowed for. Thus normal faults are rejected for the model of this earthquake. The dip angle cannot be constrained very well at this stage. Since these computations are made for a propagating point double-couple source, thrust faults dipping $\delta$ = 100° and $\delta$ = 110° correspond to the conjugate of $\delta$ = 10° and $\delta$ = 20° respectively,

and give the same amplitude ratio. Although these steep fault models cannot be discriminated from the shallow angle models on the basis of seismological data alone, the shallow angle models are more consistent with the wide lateral spread of the aftershock area.

In Fig. 6, synthetic seismograms for various depths are shown for several combinations of $\delta$ and $\lambda$ which are considered appropriate in Fig. 5. Fig. 6 shows that, for $\delta = 45°$, the amplitude ratio G2/R2 becomes too large for depths below 33 km to which depth the fault is likely to extend. Other cases for $d \leqslant 53$ km shown in Fig. 6 match the observed seismogram equally well. Thus it seems reasonable to conclude that a faulting which extends to a depth of about 50 km with a dip angle of 10–20° and a slip angle of 90° (pure thrust) to 70° (thrust with a small left-lateral component) is a good model for the Chilean earthquake. The slip angle of 45°, though not shown in Fig. 6, tends to give too small G2/R2 for most depth ranges.

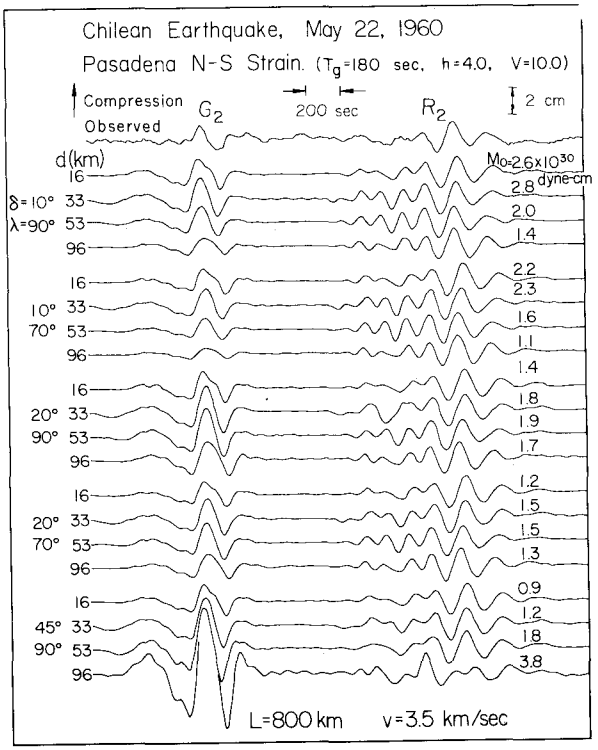


Fig. 6. Synthetic G2 and R2 for various depths. The amplitude of R2 is normalized to the observed R2 amplitude.

On the basis of this seismogram alone, it would be unreasonable to constrain these parameters any further. It should be noted, however, that the above geometry is remarkably consistent with that implied by geodetic data (Plafker, 1972), and the mechanisms and the distribution of smaller earthquakes in this area (Stauder, 1973), and the overall plate motion in this area (Le Pichon, 1968; Herron and Hayes, 1969; Morgan et al., 1969; Minster et al., 1974).

If we constrain the dip angle on the basis of well-defined spatial distribution of earthquakes in this area at 10° (Stauder, 1973; see also inset of Fig. 9), our preferred solution becomes $\delta = 10°$ and $\lambda = 90–70°$. In order to represent the slip distributed over the fault plane, the average over the three depths (16, 33, and 53 km) is taken for the case with $\delta = 10°$ and $\lambda = 90°$, and is shown in Fig. 7. If the propagation is either up-dip or down-dip, appropriate delayed average should be taken, but in view of the lack of our knowledge on the details of the propagation, only the straight sum is considered.

The most important parameter obtained in this study is the seismic moment which is determined by matching the amplitude of the synthetic seismogram with the observed seismogram. Fig. 7 shows that the appropriate value of the seismic moment is $2.7 \cdot 10^{30}$ dyn·cm, which is 3.6 times larger than that for the 1964 Alaskan earthquake, $7.5 \cdot 10^{29}$ dyn·cm, (Kanamori, 1970b), the largest value reported so far.

The width of the fault cannot be determined directly. However, if the fault extends to 50 km or so with a dip angle of 10° as suggested by the present analysis, a simple geometrical consideration would indicate a fault width of about 200 km or so (see also Fig. 9). This estimate seems consistent with the spread of the aftershock zone. With this fault width together with the fault length of 800 km and the rigidity of $7 \cdot 10^{11}$ dyn/cm$^2$, the average dislocation on the fault can be estimated as 24 m.

Although the uniqueness of the solution is not completely guaranteed, we feel that the fault parameters obtained here are fairly well constrained.

## 4. Interpretation of precursor

The interpretation of the long-period precursor shown in Figs. 1 and 3 is difficult because it is not

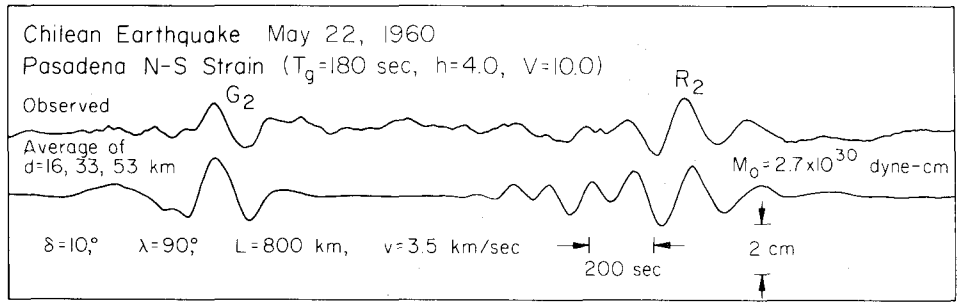


Fig. 7. The straight average of the synthetics for $d$ = 16, 33 and 53 km. The dip angle is 10° and the slip angle is 90°.

clear whether it represents direct long-period body waves or surface waves. However, whatever it may be, a very large-scale deformation is necessary to give rise to a significant signal at Pasadena, about $10^4$ km away from the source. Here, we will proceed with interpretation by assuming that this precursory signal represents direct P and S waves from the source. This assumption is based on the picture envisaged in Fig. 3. That is, the precursor is represented by a slow displacement which began at about the origin time of the foreshock, about 15 minutes before the origin time of the main shock. For such a precursory displacement, we assume a slow dislocation on a fault having a geometry similar to that of the main shock. The time function of the dislocation is given by:

$$\begin{aligned} D(t) &= 0 && t \leqslant 0 \\ D(t) &= \frac{D_0}{2}\left(1 - \cos\frac{\pi t}{\tau}\right) && 0 \leqslant t \leqslant \tau \\ D(t) &= D_0 && t > \tau \end{aligned} \qquad (1)$$

where $D_0$ is the final dislocation of the precursor and $\tau$ is the characteristic time constant, 300 – 600 sec. For the computation of the displacement field for such a slow precursor, we integrated Haskell's (1969) expressions for a homogeneous medium with P and S wave velocities of 8.0 km/sec and 4.7 km/sec, respectively. The free-surface effect is included by doubling the amplitude, and the instrument response is convolved to obtain a synthetic seismogram. Fig. 8 shows an example. Since the details of the rupture process are unknown, we assumed a bilateral propagation starting at the middle of the fault with a rupture velocity of 3 km/sec. The origin time is set at 12 min. before the origin time of the main shock, and a time constant of 450 sec is used. However, it is possible that a more gradual slip started even earlier. The details of the wave form depend on the functional form (1) and the time constant. The purpose of this comparison is to make order of magnitude estimate of such precursory displacement and to see whether the direction of the motion is consistent or not. In order to match the amplitude, a dislocation of 30 m over a fault plane of 800 × 200 km$^2$ is required. This corresponds to a seismic moment of $3.5 \cdot 10^{30}$ dyn · cm which is comparable to that of the main shock. Although the above solution is in no way unique, the fact that the same geometry as the main shock fault can explain the observed direction of the motion seems to favor the process envisaged here: a slow aseismic slip first takes place on, or on the extension of, the potential fault plane of the catastrophic event. If the precursor and the main shock took place on the same fault, the total slip would become 53 m; this value seems to be too large to be compatible with the geodetic data discussed by Plafker (1972). Plafker suggests a displacement of 20 m or so. Since the synthetic displacement at Pasadena of the precursor does not depend very much on the depth of the source, it is equally possible to match the observed precursor by an aseismic slip at depths, for example, by a slip on the downward extension of the main shock fault plane. Since the crustal deformation for such a deep source becomes very broad and is likely to escape observation, this model is preferable on the basis of the observed vertical displacement in the source area.

If we take this model, the whole sequence may be pictured as follows (Fig. 9). About fifteen minutes before the main shock a gradual slip having time constant of about 450 sec started taking place at the boundary between the downgoing oceanic lithosphere and the relatively weak asthenosphere beneath the continent. This slip caused a stress concentration at

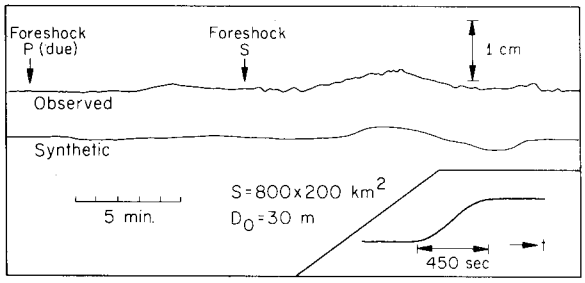


Fig. 8. Synthetic seismogram of the precursor. The inset shows the source-time function. To match the amplitude, a dislocation of 30 m is necessary over a fault plane of 800 × 200 km$^2$.

the lithosphere–lithosphere boundary above. The large foreshock may represent a brittle fracture caused by such a stress concentration. Eventually this stress concentration exceeded the breaking strength of the lithosphere–lithosphere boundary causing a major catastrophic failure, the main shock. Although this model is not a unique one, it explains the observed sequence in a consistent manner.

## 5. Discussions and conclusions

The seismic moments of the main shock and the precursor add to about $6 \cdot 10^{30}$ dyn • cm, which is nearly one order of magnitude larger than that of the Alaskan earthquake of 1964. Yet the above estimate is based on the data up to 10 minutes; it is quite possible that there may be a slip extending over an even longer period of time, hours and days. Detection of such long-time constant displacement requires reliable data on the long-period motion of the earth including free oscillations and polar motions. Previous studies show that the displacement associated with earthquakes is at least one order of magnitude too small to excite polar motions (e.g. Dahlen, 1973). However, in these estimates the upper limit of the seismic moment is set, more or less arbitrarily, at $10^{30}$ dyn • cm. The large precursory aseismic slip evidenced by the Chilean earthquake suggests that earthquakes may represent a tectonic process of much larger scale than here-to-fore considered on the basis of relatively short-period seismic waves. Earthquake may be only a part of the whole process. This possibility has already been suggested by Kanamori (1973) on the basis of tsunami earthquakes in which aseismic slip plays an important role in the entire earthquake process. Shimazaki (1974) shows that, in northern Japan, a preseismic slip extends to a depth of 100 km where brittle fractures are unlikely to take place. The present model is consistent with this finding. Thatcher (1974) also suggests, on the basis of geodetic data, that the 1906 San Francisco earthquake may be associated with considerable aseismic slip at depths. Dziewonski and Gilbert (1974) suggest a slow precursory deformation before large deep-focus earthquakes. In view of these results, the possible role of earthquakes in the global problems of the earth such as polar motion, spatial and temporal plate motion, etc., deserves further investigation (Anderson, 1974).

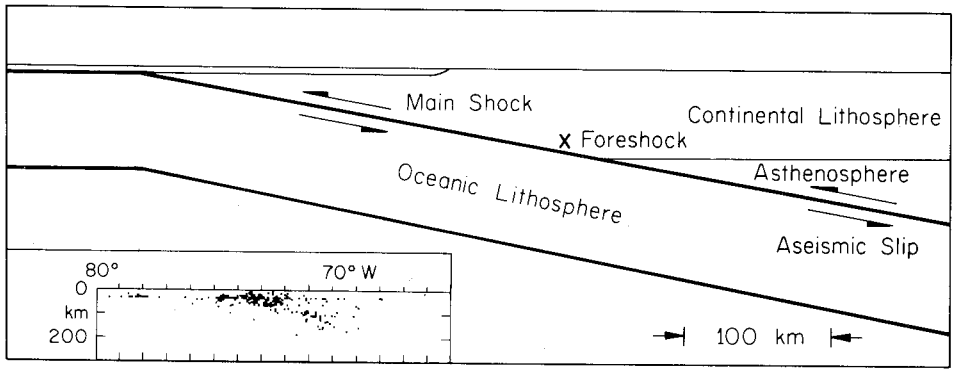


Fig. 9. Schematic figure illustrating the proposed focal process of the Chilean earthquake of 1960. First, aseismic slip takes place along the lithosphere–asthenosphere boundary at depths. Small foreshock is triggered by the stress concentration caused by this aseismic slip. Finally, the upper lithosphere–lithosphere boundary breaks as the catastrophic main shock. The inset shows the vertical cross-section of the seismicity in this area given by Stauder (1973).

If the precursory displacement discussed here is characteristic of at least a certain class of earthquakes, it will have an obvious importance in earthquake prediction and earthquake hazard reduction. An even relatively short-time constant (e.g., 10 minutes) precursor would still be useful in allowing people to take some preventive measures. For several Japanese earthquakes (e.g. Ajigasawa earthquake, 1793; Sado earthquake, 1802; Hamada earthquake, 1872), premonitory land upheavals were reported to have taken place several minutes to several hours before the earthquake (Imamura, 1930; see also Kanamori, 1973). However, these results are based on either descriptions in old literature or interviews with eyewitnesses; none of these upheavals has been observed by instruments, and objective evaluation of these data is extremely difficult. The precursory slip of the Chilean earthquake may represent an instrumental verification of such observations. Since the main shock of the Chilean earthquake itself is larger by far than any other event, it is possible that the associated displacement was also larger by far than others so that it was marginally detectable. If this is the case, smaller events may also be preceded by some aseismic slip which is proportionally small so that it has not been detected by ordinary instrumentation. It seems possible that improved and strategically deployed instrumentation in the future will make detection of this type of precursory displacement possible for smaller events.

The present interpretation of the precursor depends entirely on the Pasadena strain record. Although the signal looks very significant, there is still a slim possibility that it was caused by some instrumental instability, and further study is obviously desirable.

## Acknowledgment

We thank Don Anderson for kindly reading the manuscript, and Frank Press for kindly suggesting to us the use of the Benioff 1–90 system for the calibration of the strain instrument. Francis Lehner provided us with useful information concerning the instrument characteristics.

This research was partially supported by National Science Foundation grant GA 40752 and the Advanced Research Projects Agency of the Department of Defence and was monitored by the Air Force Office of Scientific Research under contract No. F44620-72-C-0078.

## References

Alsop, L.E., 1964. Bull. Seismol. Soc. Am., 54: 755–776.
Alsop, L.E., Sutton, G.H. and Ewing, M., 1961. J. Geophys. Res., 66: 631–641.
Alterman, Z., Jarosch, H. and Pekeris, C.L., 1959. Proc. R. Soc. London, Ser. A, 252: 80–95.
Anderson, D.L., 1974. Science, 186: 49–50.
Benioff, H., 1935. Bull. Seismol. Soc. Am., 25: 283–309.
Benioff, H., Press, F. and Smith, S.W., 1961. J. Geophys. Res., 66: 605–619.
Ben-Menahem, A., 1961. Bull. Seismol. Soc. Am., 51: 401–435.
Ben-Menahem, A., 1965. J. Geophys. Res., 70: 4641–4651.
Ben-Menahem, A., 1971. Geophys. J.R. Astron. Soc., 25: 407–417.
Ben-Menahem, A., Smith, S.W. and Teng, T.L., 1965. Bull. Seismol. Soc. Am., 55: 203–235.
Ben-Menahem, A., Rosenman, M. and Harkrider, D.G., 1970. Bull. Seismol. Soc. Am., 60: 1337–1387.
Bogert, B.P., 1961. J. Geophys. Res., 66: 643–646.
Dahlen, F.A., 1973. Geophys. J., 32: 203–217.
Dziewonski, A.M. and Gilbert, F., 1974. Nature, 247: 185–188.
Haskell, N.A., 1969. Bull. Seismol. Soc. Am., 59: 865–908.
Herron, E.M. and Hayes, D.E., 1969. Earth and Planet. Sci. Lett., 6: 77–83.
Hodgson, J.H. and Wickens, A.J., 1965. Publ. Dom. Obs., Ottawa, Ont., 31: 123.
Imamura, A., 1930. Publ. Earthquake Invest. Comm. Foreign Lang., 25: 1–143.
Kanamori, H., 1970a. J. Geophys. Res., 75: 5011–5027.
Kanamori, H., 1970b. Phys. Earth Planet. Inter., 2: 259–275.
Kanamori, H., 1970c. J. Geophys. Res., 75: 5029–5040.
Kanamori, H., 1973. In: F.A. Donath (Editor), Annual Review of Earth and Planetary Science, 1: 213–239. Annual Reviews Inc., Palo Alto.
Le Pichon, X., 1968. J. Geophys. Res., 73: 3661–3697.
Minster, J.B., Jordan, T.H., Molnar, P. and Haines, E., 1974. Geophys. J.R. Astron. Soc., 36: 541–576.
Morgan, W.J., Vogt, P.R. and Falls, D.F., 1969. Nature, 222: 137–142.
Ness, N.F., Harrison, J.C. and Slichter, L.B., 1961. J. Geophys. Res., 66: 621–629.
Plafker, G., 1972. J. Geophys. Res., 77: 901–925.
Plafker, G. and Savage, J.C., 1970. Geol. Soc. Am. Bull., 81: 1001–1030.
Press, F., Ben-Menahem, A. and Toksöz, M.N., 1961. J. Geophys. Res., 66: 3471–3485.
Saito, M., 1967. J. Geophys. Res., 72: 3689–3699.
Shimazaki, K., 1974. Phys. Earth Planet. Inter., 8: 148–157.
Stauder, W., 1973. J. Geophys. Res., 78: 5033–5061.
Thatcher, W., 1974. EOS, 55: 426 (abstract).

## Appendix

The excitation of free-oscillations has been studied by many investigators. Here we modify Saito's (1967) formulations by using the fault representations given by Ben-Menahem et al. (1965), so that the final expressions can be given in a form analogous to those given by Ben-Menahem et al. (1970) for long-period surface waves. We take spherical coordinates $(r, \theta, \phi)$ with the origin at the earth's center. After somewhat lengthy but straightforward algebra, we have, for the transverse component of torsional oscillations excited by a point double-couple at $r = r_s$ on the polar axis, varying stepwise in time (unit moment):

$$U_\phi(\vec{r}, t) = \sum_n y_1(r) \cos \sigma_n t \left( -L_1 q_L \frac{dP_n^1}{d\theta} + L_2 p_L \frac{dP_n^2}{d\theta} \right) \quad (2)$$

where $t$ is time measured from the origin time; $\sigma_n$ is the $n$-th eigen angular frequency; $P_n^m$ is the associated Legendre function. Here:

$$q_L = -(\cos \lambda \cos \delta) \sin \phi + (\sin \lambda \cos 2\delta) \cos \phi \quad (3)$$

$$p_L = (\sin \lambda \sin \delta \cos \delta) \sin 2\phi + (\cos \lambda \sin \delta) \cos 2\phi \quad (4)$$

$$L_1 = \frac{(2n+1)}{4\pi\sigma_n^2 n(n+1) I_1 r_s} \frac{r_s}{\mu_s} y_2(r_s)$$

$$L_2 = L_1 \frac{\mu_s}{r_s} \frac{y_1(r_s)}{y_2(r_s)}$$

where $\lambda$ and $\delta$ are the slip angle and the dip angle of the fault as defined by Ben-Menahem et al. (1965; see Fig. 10), and $\mu_s$ is the rigidity at the source depth; $y_1$ and $y_2$ are respectively the radial factors of displacement and stress of the $n$-th normal mode, and $I_1$ is the energy integral as defined in Alterman et al. (1959). In the above $q_L$ and $p_L$ are identical to those defined by Ben-Menahem et al. (1970), and are determined by fault geometry; $L_1$ and $L_2$ are calculated from the eigenfunctions and the source depth, and are independent of the source geometry. Once $y_1(r), y_2(r), I_1$ and $\sigma_n$ are computed for various normal modes, the displacement can be easily computed for any fault geometry by eq. 2 by a superposition of the normal modes. The expression for the radial component can be obtained similarly.

Likewise, the vertical component of spheroidal oscillations can be given by:

$$U_r(\vec{r}, t) = \sum_n y_1(r) \cos \sigma_n t \ (K_o s_R P_n^o - K_1 q_R P_n^1 + K_2 p_R P_n^2) \quad (5)$$

where:

$$s_R = \sin \lambda \sin \delta \cos \delta \quad (6)$$

$$q_R = \sin \lambda \cos 2\delta \sin \phi + \cos \lambda \cos \delta \cos \phi \quad (7)$$

$$P_R = \cos \lambda \sin \delta \sin 2\phi - \sin \lambda \cos \delta \cos 2\phi \quad (8)$$

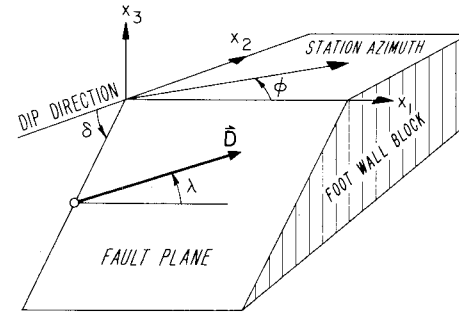


Fig. 10. Fault representation of Ben-Menahem et al. (1965: slightly modified). Vector $\vec{D}$ is the slip vector and gives the displacement of the hanging wall block. The slip angle $\lambda$ is measured counter-clockwise from the positive $x_1$-direction. The dip angle $\delta$ is measured from the negative $x_2$- axis. The azimuth $\phi$ is measured, from $x_1$- axis, counter-clockwise. For the Chilean earthquake, $x_1$-axis coincides with N10°E direction.

$$K_o = \frac{2n+1}{4\pi\sigma_n^2 [I_1 + n(n+1) I_2] r_s} \frac{2(3\lambda_s + 2\mu_s)}{\lambda_s + 2\mu_s} \cdot$$

$$\left[ y_1(r_s) - \frac{r_s}{3\lambda_s + 2\mu_s} y_2(r_s) - \frac{n(n+1)}{2} y_3(r_s) \right]$$

$$K_1 = \frac{2n+1}{4\pi\sigma_n^2 [I_1 + n(n+1) I_2] r_s} \frac{r_s}{\mu_s} y_4(r_s)$$

$$K_2 = \frac{2n+1}{4\pi\sigma_n^2 [I_1 + n(n+1) I_2] r_s} y_3(r_s)$$

In the above, $y_1(r)$ and $y_3(r)$ are the radial factors of displacements, and $y_2(r)$ and $y_4(r)$ are the radial factors of stresses; $I_1$ and $I_2$ are energy integrals. These are defined in Alterman et al. (1959). $\lambda_s$ is the Lame elastic constant at the source depth.

The radial component of the displacement is given by:

$$U_\theta(r, t) = \sum_n y_3(r) \cos \sigma_n t \left[ K_o s_R \frac{dP_n^o}{d\theta} - K_1 q_R \frac{dP_n^1}{d\theta} + K_2 p_R \frac{dP_n^2}{d\theta} \right] \quad (9)$$

In the above $s_R$, $q_R$ and $p_R$ are identical to those defined by Ben-Menahem et al. (1970), and are determined by the fault geometry; $K_o$, $K_1$ and $K_2$ depend on the eigenfunctions and the source depth, and are independent of the source geometry.

The expressions for the transverse component can be obtained similarly.